



# Highly selective oxidation of glucose to formic acid over synthesized hydrotalcite-like catalysts under base free mild conditions

Hülya A. Kılıç<sup>1</sup> · Emre Kılıç<sup>1</sup> · Lütfi Erden<sup>1</sup> · Yaşar Gök<sup>1</sup>

Received: 12 January 2022 / Accepted: 7 August 2022 / Published online: 16 August 2022  
© The Author(s), under exclusive licence to Springer Nature B.V. 2022

## Abstract

Sustainable and renewable production of platform chemicals and fuels has been gradually rising. Formic acid is one of the important chemicals for leather, cosmetic and pharmaceutical industries as well as hydrogen source. In this study, selective oxidation of biomass-derived glucose to formic acid was investigated under base free medium at 70 °C over synthesized hydrotalcite-like catalysts using hydrogen peroxide as oxidant. Effect of Mg/Al ratio (6/1, 3/1, 1/1, 1/3 and 1/6) and heat treatment (drying and calcination) on catalyst structure and product distributions; effect of calcination temperature (450, 650 and 900 °C), solvent composition (ethanol/water) and reaction temperature (30, 50 and 70 °C) on catalytic activity and product selectivity were investigated. Reducing the Mg/Al ratio enhanced the density of metal-OH bonds, surface area and uniformity of pores up to some extent. The highest glucose conversion and formic acid selectivity were achieved over Mg–Al (1:3) catalyst as 38.7 and 99.0%, respectively. The calcined catalysts (at 450 °C) exhibited 7 times higher selectivities and 4 times higher activities than the dried ones. However, higher calcination temperatures did not show remarkable increments in activities and yields. Easily prepared, cheap Mg–Al (1:3) catalyst provided promising results even at low temperature with hydrogen peroxide at atmospheric medium in a low boiling point solvent (ethanol).

---

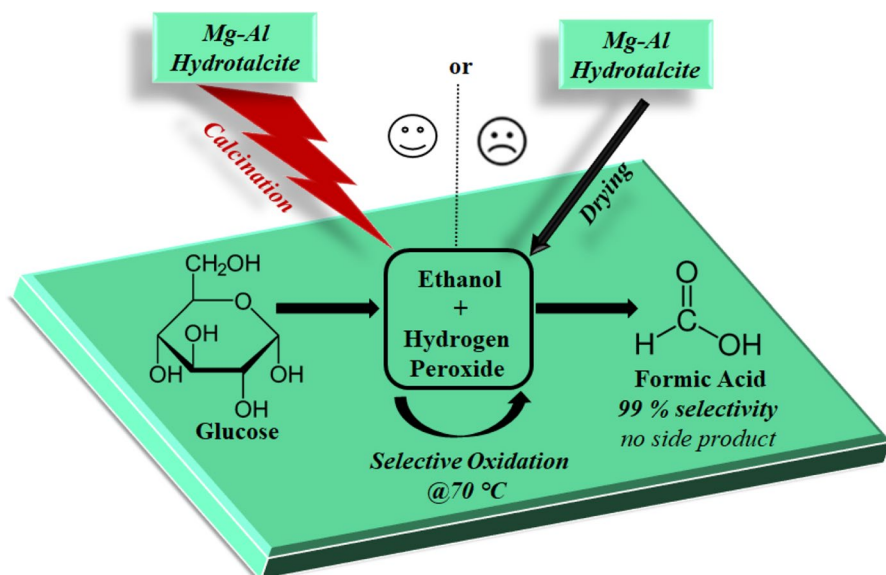
Hülya A. Kılıç, Emre Kılıç, Lütfi Erden and Yaşar Gök have contributed equally.

---

✉ Emre Kılıç  
emre.kilic@usak.edu.tr

<sup>1</sup> Department of Chemical Engineering, Uşak University, 64200 Uşak, Turkey

## Graphical abstract



**Keywords** Formic acid · Glucose · Oxidation · Hydrotalcite · Biomass

## Introduction

The global market of formic acid (FA) has been steadily increasing since it is one of the efficient platform chemicals used in the food, textile and leather, pharmaceutical, and cosmetic industries [1]. Formic acid can be transported easily due to its stability at room conditions, nontoxic and nonflammable properties [2]. FA has a crucial role as a hydrogen donor [3] as decomposes easily to produce hydrogen and carbon dioxide above 140 °C [4–6]. This makes it favorable, safe, and economic feedstock to be used in fuel cells and many hydrogenation reactions.

Although many different methods have been applying for lab-scale production of formic acid [7–10], today two main non-renewable methods have been using for large-scale. These two methods are hydrolysis of methyl formate and carbonylation of methanol [11]. The methyl formate process is still the most widely used method since 90% of formic acid is produced industrially by this reaction. However, high process costs and the formation of undesired products along with formic acid push people to find sustainable, renewable, and cost-effective methods.

The conversion of biomass-derived molecules to fuels, especially formic acid is attractive in the last years [12–21]. Two different chemical strategies are present for glucose transformation to formic acid; dehydration-hydrolysis and oxidation. The dehydration-hydrolysis process consists of dehydration of glucose to 5-hydroxymethylfurfural [22–27] that is followed by its rehydration to formic and

levulinic acids (LA) [22, 28–31]. The formation of LA together with FA limits the thermodynamic yields of these acids [28]. Nowadays, extensive efforts have been making for highly selective glucose oxidation to formic acid [14, 21, 32, 33].

Glucose oxidation to FA occurs under basic conditions or over base sites of the catalysts [14, 32]. Wide range of homogeneous and heterogeneous catalysts, different O<sub>2</sub> sources, different reaction mediums, and conditions were investigated in the literature [12–15, 34–37]. Wang et al. (2019) achieved 91.3% formic acid yield with LiOH at room temperature for 8 h by using H<sub>2</sub>O<sub>2</sub> as an oxidant [14]. Jin et al. (2008) investigated the fast oxidation of glucose to formic acid with H<sub>2</sub>O<sub>2</sub> in the presence of an alkali medium (NaOH) at 250 °C. Formic acid formed only in 60 s in 75% FA yield [32]. Albert et al. (2012) reported oxidation of biomass (xylan) conversion to formic acid with Keggin-type polyoxometalate (H<sub>5</sub>PV<sub>2</sub>Mo<sub>10</sub>O<sub>40</sub>) as a homogeneous catalyst by using p-toluenesulfonic acid as an additive at 90 °C and 30 bar O<sub>2</sub>. The formic acid yield was obtained as 53% for 24 h [38]. However, it is still a great challenge to carry out the glucose oxidation process providing a high yield of formic acid under base-free and mild conditions.

Hydrotalcites (HTs), called layered double hydroxides, are natural minerals containing M<sup>+2</sup> and M<sup>+3</sup> metal oxides [39, 40]. They can be synthesized from basic metal salts by co-precipitation easily. HTs have a high amount of hydroxyl groups and surface basic sites which make them active and selective oxidation catalysts [40]. Promising catalytic performances of this type of catalyst were reported many times [40–47]. Sato et al. [43] brought a unique perspective to hydrotalcite type catalysts for selective formic acid production via oxidation of glucose. They calcined Mg–Al type hydrotalcite (HT) and tested in glucose oxidation in ethanol medium. Although satisfactory glucose conversion was obtained over uncalcined HT, calcination significantly improved the formic acid selectivity (upto 78.1% with complete glucose conversion). In comparison with the other common catalysts, -such as mono alkali oxides (MgO and CaO), zeolites (H-ZSM-5 and H-β) and SiO<sub>2</sub>- the highest yield was achieved over calcined HT.

The present work focused on the performance of different Mg–Al type hydrotalcite catalysts on glucose oxidation. HTs were synthesized by the co-precipitation method. These catalysts were tested in selective glucose oxidation to formic acid. Effect of Mg/Al ratio, thermal process, reaction temperature, and solvent composition on catalytic activity and formic acid selectivity were investigated under base-free mild conditions.

## Experimental study

### Materials

Glucose, magnesium nitrate hexahydrate (≥99%), aluminum nitrate nanohydrate (≥99%), and sodium hydroxide (97%) were purchased from Merck KGaA (Darmstadt, Germany). Sodium carbonate anhydrous (99%) and hydrogen peroxide (35%) were supplied by Isolab Chemicals (Wertheim, Germany).

## Catalyst preparation

### Synthesis of hydrotalcite-like catalysts with different Mg–Al ratios

Mg–Al hydrotalcites were prepared by a co-precipitation method. Solution A was prepared by dissolving the magnesium nitrate hexahydrate  $[\text{Mg}(\text{NO}_3)_2 \cdot 6\text{H}_2\text{O}]$  and the aluminum nitrate nonahydrate  $[\text{Al}(\text{NO}_3)_3 \cdot 9\text{H}_2\text{O}]$  in water. Solution B was aqueous solution of 1 M NaOH. These two solutions were simultaneously added into aqueous sodium carbonate ( $\text{Na}_2\text{CO}_3$ ) solution at 60 °C and pH 10. After consumption of the metal solutions, the mixture was stirred for 1 h and left to mature for 18 h. The resulting precipitates were filtered, washed with deionized water, dried at 110 °C for 18 h, and calcined at 450 °C for 5 h with a heating rate of 10 °C/min. The synthesized hydrotalcites are labeled Mg–Al( $x:y$ ) ( $x:y$  = Mg/Al ratio). The Mg–Al(3:1) catalyst was also calcined at 650 and 900 °C with the same heating rate, time and labeled as Mg–Al(3:1)-650 and Mg–Al(3:1)-900, respectively.

### Characterization of catalysts

The crystal phases and X-ray diffraction (XRD) patterns of the catalysts were analyzed with the Rigaku Smartlab instrument. The patterns were scanned between  $2\theta=5\text{--}80^\circ$  angles where the scanning speed was  $3^\circ/\text{s}$ . A wavelength of  $\lambda=0.15418$  nm and a power of 45 kV/40 mA of Cu  $K\alpha$  beam source were used. FT-IR measurements of the catalysts were made with Perkin-Elmer Brand Paragon 1000 model Fourier Transform Infrared Spectroscopy (FT-IR/ATR). Measurements were taken with a powder sample between 400 and  $4000\text{ cm}^{-1}$ . Nitrogen physisorption analyzes were performed with the Quantachrome Autosorb IQ2 model instrument. All samples were degassed at 120 °C for 8 h prior to adsorption. The multipoint adsorption data were obtained at 77 K and relative pressure of 760 mmHg. The surface area, pore structures, and pore volumes of the catalysts were determined by the BET method.

### Catalyst screening tests

Synthesized catalysts were tested in glucose oxidation. Oxidation tests were carried out at 70 °C for 6 h in both water and ethanol medium. Hydrogen peroxide solution (35%) was used as an oxidant.

The reactions were performed in a reflux glass bubble reactor with a volume of 100 ml. A specified amount of catalyst and glucose were loaded into the reactor. This was followed by the addition of oxidant in 50 ml of solvent. The solution was

stirred at 500 rpm under heating in an oil bath on the magnetic stirrer. Each sample, taken at every two hours, was cooled immediately in an ice bath, filtered with a 0.45  $\mu\text{m}$  PVDF syringe filter, diluted for HPLC analysis.

### Parametric studies

Parametric studies were performed with the most efficient catalyst (providing the highest conversion and FA selectivity). The effects of calcination temperatures (450  $^{\circ}\text{C}$ , 650  $^{\circ}\text{C}$ , and 900  $^{\circ}\text{C}$ ), solvent compositions (ethanol, water, ethanol/water: 50/50 (v/v)), reaction temperatures (30  $^{\circ}\text{C}$ , 50  $^{\circ}\text{C}$ , and 70  $^{\circ}\text{C}$ ) and catalyst/glucose ratios (1/1, 1/2 and 1/5) on glucose oxidation were investigated in order to optimize the reaction parameters.

### Recyclability test

Recyclability of the catalysts was performed in the same reaction medium. After each run, used catalyst was washed, dried and calcined at 450  $^{\circ}\text{C}$  and used in the consecutive cycle. Used catalyst after the 1st run was analyzed by XRD.

### Product analysis

The diluted samples were analyzed by Thermo Ultimate 3000 model high pressure liquid chromatography (HPLC) equipped with ICsep Coregel 87H3 (300  $\times$  7.8 mm) organic acid column, UV-Visible (UV-Vis), and Refractive Index (RI) detectors. The injection volume was 20  $\mu\text{l}$ . Dilute sulfuric acid (8 mM) was used as the mobile phase. The flow rate was 0.6 ml/min, the column temperature was 60  $^{\circ}\text{C}$  and the RID temperature was 45  $^{\circ}\text{C}$ . Organic acids (formic acid, acetic acid, levulinic acid) concentrations were determined by UV-Vis detector while sugar (glucose and fructose) concentrations by RID detector.

Glucose conversion (X), product carbon-yield (Y) and carbon-selectivity (S) were calculated using the following equations.

$$X(\%) = \frac{\text{Moles of Glucose}_{\text{in}} - \text{Moles of Glucose}_{\text{out}}}{\text{Moles of Glucose}_{\text{in}}} \times 100$$

$$Y(\%) = \frac{\text{Moles of the Product} \cdot \text{Number of Carbon in the Product}}{\text{Moles of Glucose}_{\text{in}} \times 6} \cdot 100$$

$$S(\%) = \frac{\text{Moles of the Product} \cdot \text{Number of Carbon in the Product}}{\text{Moles of Glucose Reacted} \times 6} \cdot 100$$

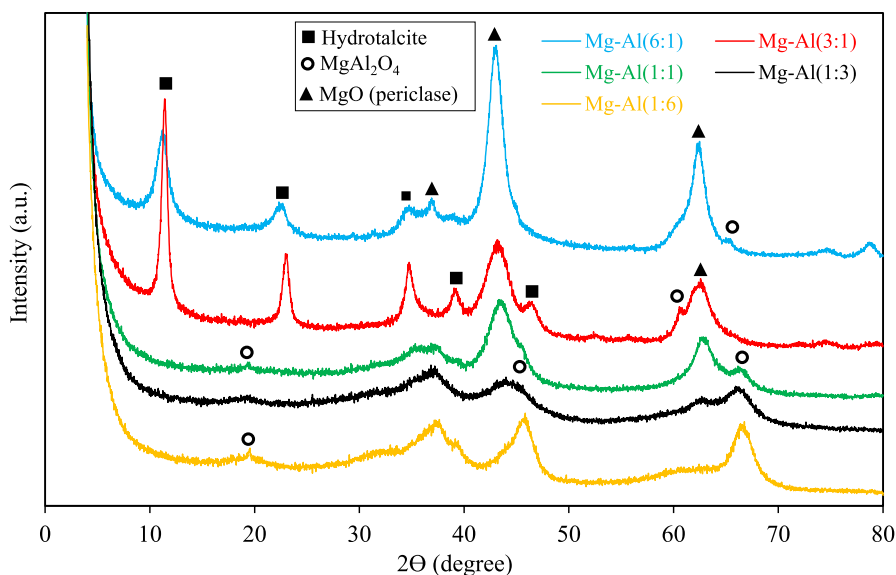


Fig. 1 XRD patterns of calcined hydrotalcite-like structures at different Mg/Al ratios

## Results and discussion

### Characterization of the synthesized catalysts

The XRD patterns of calcined hydrotalcite-like structures with different Mg/Al ratios are demonstrated in Fig. 1. It was observed that each catalyst was compatible with the literature in terms of Mg/Al ratios [44, 48]. Mg–Al(6:1) catalyst had three different crystal phases which were hydrotalcite ( $2\theta=12^\circ$ ,  $23^\circ$ ,  $35^\circ$ ), magnesium-aluminate ( $2\theta=65^\circ$ ) and magnesium oxide/periclase ( $2\theta=37^\circ$ ,  $43^\circ$ ,  $63^\circ$ ). The Mg–Al(3:1) had high-density hydrotalcite crystal phases ( $2\theta=12^\circ$ ,  $23^\circ$ ,  $35^\circ$ ,  $40^\circ$ , and  $47^\circ$ ) and less magnesium oxide/periclase crystals ( $2\theta=43^\circ$  and  $63^\circ$ ). Pure hydrotalcite crystal structure forms when the weight ratio of Mg/Al is between 2–4% [49]. It was realized from the XRD patterns, the density of hydrotalcite crystal phases decreased outside of this range. For Mg–Al(1:1), the magnesium-aluminate ( $2\theta=20^\circ$  and  $65^\circ$ ) crystallinity was very low but magnesium oxide/periclase ( $2\theta=37^\circ$ ,  $43^\circ$ ,  $63^\circ$ ) crystallinity was high. Mg–Al(1:3) had low crystallinity or smaller crystals ( $<5$  nm) so it could not be detected by XRD analysis. The crystal phases of Mg–Al(1:3), were magnesium-aluminate ( $2\theta=44^\circ$ ,  $63^\circ$ , and  $65^\circ$ ) and magnesium oxide/periclase ( $2\theta=37^\circ$ ). Mg–Al(1:6) catalyst had a high crystal density of magnesium-aluminate ( $2\theta=20^\circ$ ,  $45^\circ$ , and  $65^\circ$ ) and low crystal density of magnesium oxide/periclase ( $2\theta=37^\circ$ ). When the Mg/Al ratio of the catalysts decreased (from the ratio Mg/Al = 3), the hydrotalcite crystals were disappeared and the density of magnesium-aluminate crystals increased.

The high-temperature X-ray diffraction analysis was performed at different temperatures to observe the differences in the diffraction planes of uncalcined

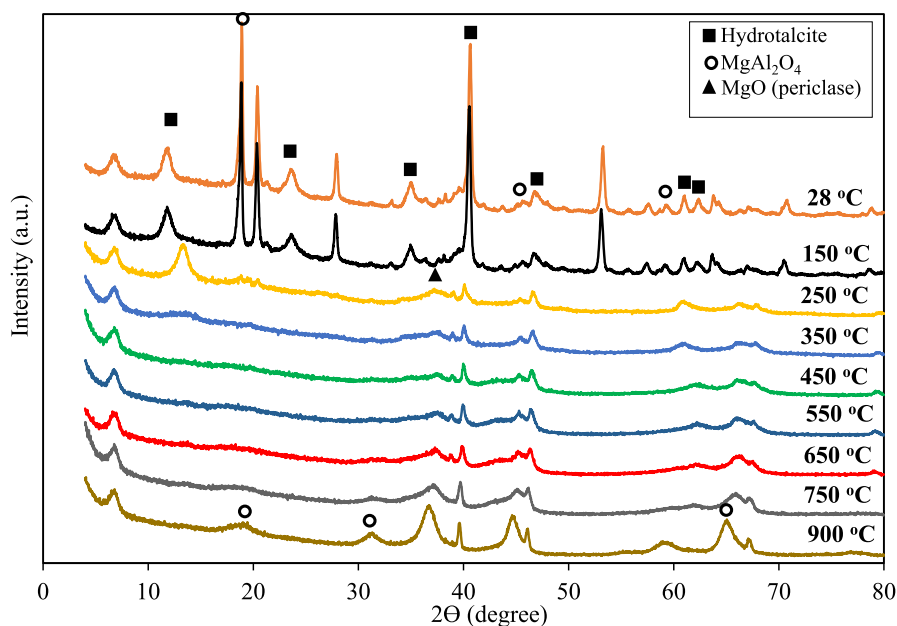


**Fig. 2** XRD patterns of Mg–Al (3:1) HT catalyst at different temperatures

Mg–Al(3:1). The XRD patterns of this catalyst are shown in Fig. 2. Dense crystallinity was clearly visible in the patterns at room temperature and 150 °C. As seen in Fig. 2, there were hydrotalcite crystals in Mg–Al (3:1) structure at these two temperatures. When the temperature reached 250 °C, the intensity of the crystal peaks decreased. At 350 °C the crystal structure of the catalyst transformed into an amorphous structure. There was no change in crystal density up to 900 °C. Dense magnesium aluminate crystal phases were noticed at 20°, 32°, 59°, and 65° at 900 °C. As a result, when the temperature increased, the hydrotalcite

**Table 1** Textural properties of hydrotalcite-like catalysts

Catalysts	BET surface area (m <sup>2</sup> /g)	B.J.H. Pore diameter (nm)	Pore volume (cm <sup>3</sup> /g)	External surface area (m <sup>2</sup> /g)
Mg–Al(1:6)	189	9.50	0.448	189
Mg–Al(1:3)	232	7.07	0.411	232
Mg–Al(1:3)-D	57.6	24.5	0.353	57.6
Mg–Al(1:1)	124	17.4	0.542	120
Mg–Al(3:1)	64.7	20.0	0.324	64.7
Mg–Al(3:1)-650	93.1	34.1	0.793	93.1
Mg–Al(3:1)-900	93.4	36.7	0.858	90.1
Mg–Al(6:1)	52.8	12.9	0.170	52.8

structure of synthesized material changed and its crystal structure tended toward amorphous.

Textural properties of the prepared hydrotalcite-like catalysts are given in Table 1. It was observed that there was a steady increase in specific surface area with the decrease in the Mg/Al ratio (up to 1:6). This increment was 20% between catalysts possessing hydrotalcite structure which was almost % 90 in catalysts having mostly magnesium–aluminum oxide structure. By increasing the calcination temperature of Mg–Al(3:1) from 450 to 650 °C, the surface area and pore diameter were improved by almost 50%, while the pore volume more than doubled. However, the structure of this catalyst did not change significantly when the calcination temperature raised to 900 °C. Effect of calcination process on textural properties is clearly noticeable in Mg–Al(1:3). Calcination highly increased the surface area of this sample.

Nitrogen adsorption–desorption isotherms and pore size distributions of the synthesized catalysts are given in Figs. 3 and 4. All of the catalysts indicated Type IV isotherm with distinct Type H3 hysteresis loop which implies mesoporous character, slit-shaped pores, wide pore size distribution, and high energy of adsorption [50]. Most of the pores are distributed in the mesopore range. Few amounts of macropores were observed.

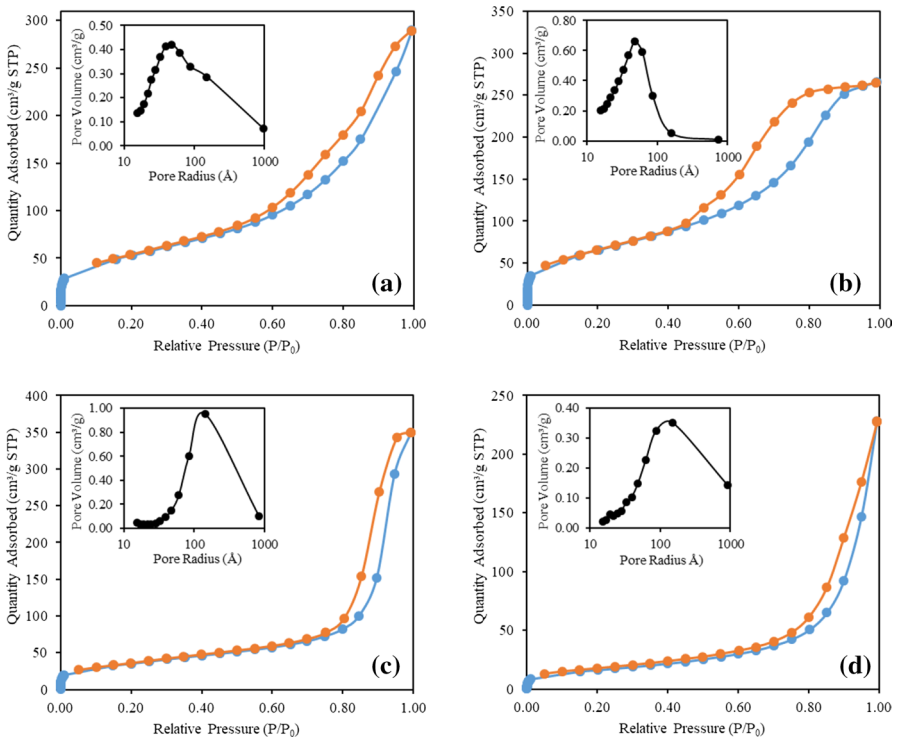


**Fig. 3** N<sub>2</sub> Adsorption and desorption isotherms of hydrotalcite-like catalysts **a** Mg–Al(1:6) **b** Mg–Al(1:3) **c** Mg–Al(1:1) **d** Mg–Al(1:3)



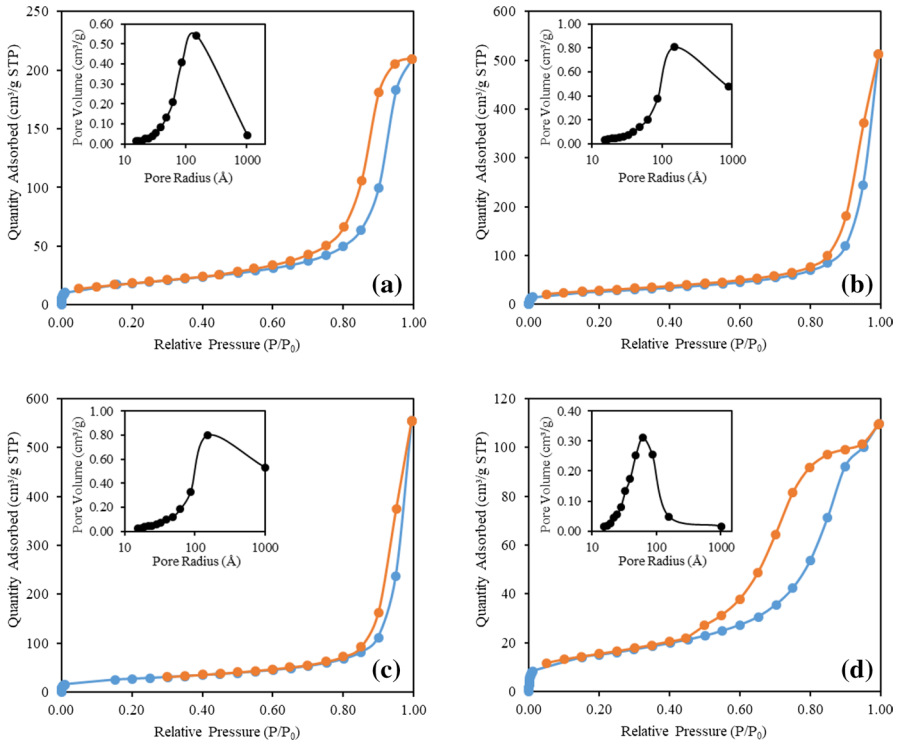


**Fig. 4** N<sub>2</sub> Adsorption and desorption isotherms of hydrotalcite-like catalysts **a** Mg–Al(3:1) **b** Mg–Al(3:1)-650 **c** Mg–Al(3:1)-900 **d** Mg–Al(6:1)

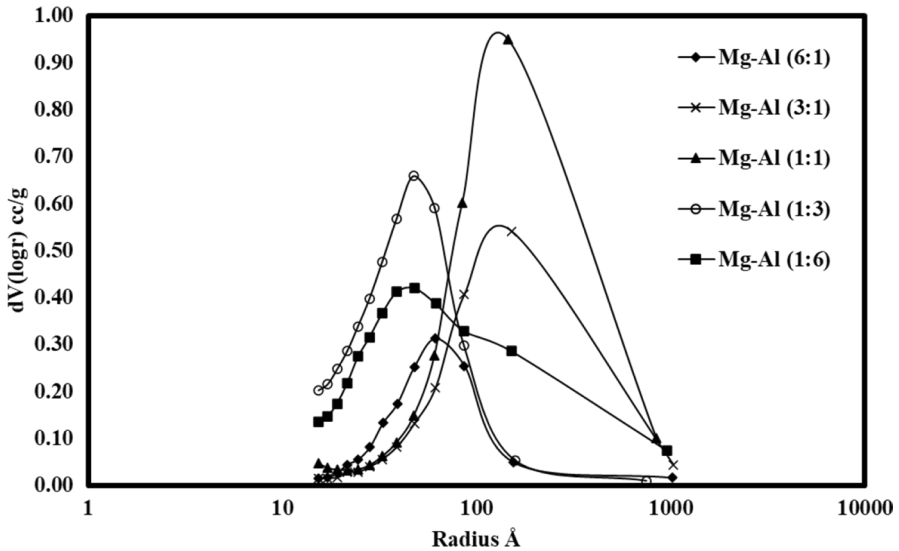


**Fig. 5** BJH Pore size distributions of catalysts with different Mg–Al ratio

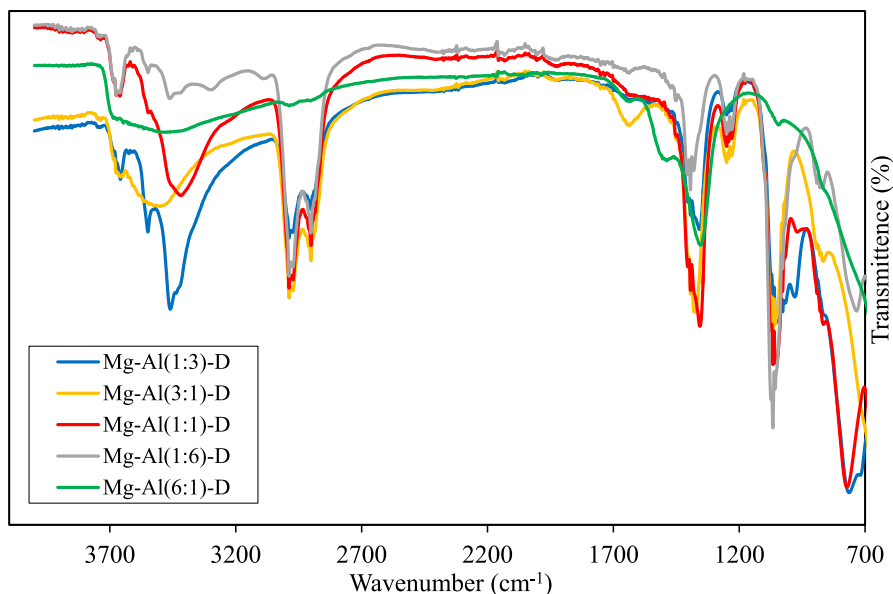


**Fig. 6** FT-IR spectra of dried hydrotalcite-like catalysts

The Mg–Al (1:3) exhibited the most narrow pore size distribution on lower mesopore region, whereas the distributions patterns of other catalysts were much broader. This suggests that Mg–Al (1:3) was more uniformly packed together compared to others (Fig. 5).

The FT-IR spectra of dried hydrotalcite-like structures at different Mg/Al ratios are given in Fig. 6. Each catalyst is compatible with the literature [51, 52]. The absorption band at  $3698\text{ cm}^{-1}$  was stretching vibrations of metal-OH (such as Mg-OH and Al-OH) bonds which was seen in Mg–Al(1:1), Mg–Al(1:3), and Mg–Al(1:6) materials. In these regions, Lewis acid centers formed on the aluminum side, and both basic and oxidizing centers formed on the Mg side. This band is not found in Mg–Al(3:1) and Mg–Al(6:1) catalysts [14, 34]. Absorption bands at  $3400\text{--}3500\text{ cm}^{-1}$  formed by physisorption between located interphase and metal-O–H bonds. The sharp absorption bands at  $2980\text{ cm}^{-1}$  were caused by the  $\text{CO}_3^{2-}\text{-H}_2\text{O}$  stretching vibrations [51] formed by the hydrogen bonding of carbonate ions attached to the Mg–Al structure [53]. Also,  $1350\text{--}1380\text{ cm}^{-1}$  bands were caused by  $\text{CO}_3^{2-}$  in the structure. The band at  $1646\text{ cm}^{-1}$  observed in Mg–Al(3:1) was H–O..H vibrations by the presence of crystalline water. The bands obtained at  $1250$  and  $1066\text{ cm}^{-1}$  were the symmetric-asymmetric stretching movements of the ether groups.

FT-IR spectra of calcined catalysts at different Mg/Al ratios are shown in Fig. 7. The intensity of metal-OH bonds (absorption band at  $3698\text{ cm}^{-1}$ ) in Mg–Al(1:1) decreased after the calcination process, but it remained constant in Mg–Al(1:3) and Mg–Al(1:6) catalysts. In Mg–Al(3:1) and Mg–Al(6:1) catalysts, the intensity of these bonds reduced dramatically with calcination. Sharp absorption bands

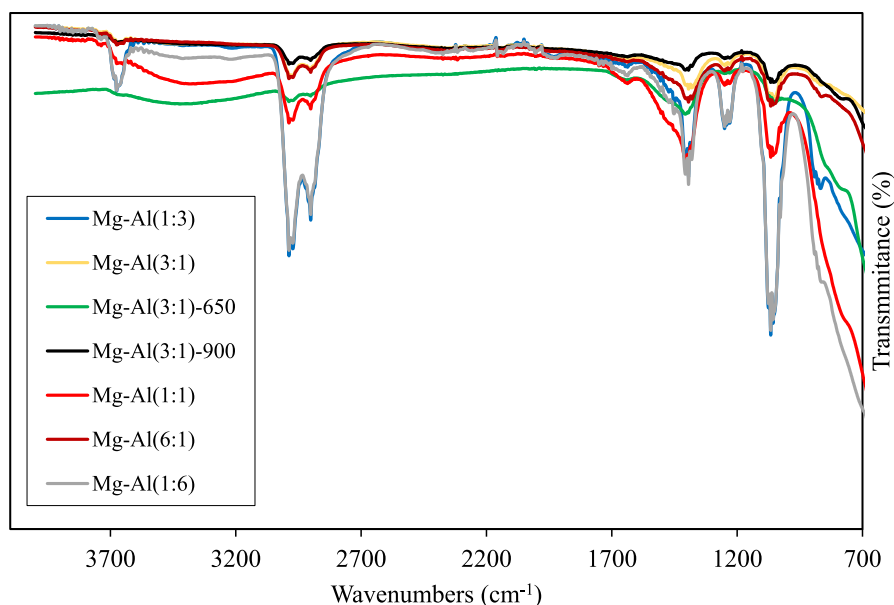


**Fig. 7** FT-IR spectra of calcined hydrotalcite-like catalysts

( $\text{CO}_3^{2-}\text{-H}_2\text{O}$  stresses) at 2901 and 2980  $\text{cm}^{-1}$  maintained their intensity in Mg-Al(1:3) and Mg-Al(1:6), which decreased significantly in other catalysts as a result of calcination. For these catalysts, similar results were obtained at 1390, 1250, and 1066  $\text{cm}^{-1}$  ( $\text{CO}_3^{2-}$  in the structure). Mg-Al(1:1) also maintained its intensity at 1390  $\text{cm}^{-1}$ . As a result, reactive metal-OH and  $\text{CO}_3^{2-}$  groups were preserved as crystal structures getting closer to magnesium-aluminate even if catalysts were exposed to calcination. FT-IR spectra of different calcination temperatures (650 °C and 900 °C) of Mg-Al(3:1) are also shown in Fig. 7. In the structure, the metal oxides absorption bands remained at the same level but others decreased to negligible levels.

## Glucose conversion tests

### Activity test of dried hydrotalcite-like catalysts

The glucose conversions over dried hydrotalcite-like catalysts with different Mg/Al ratios (6/1, 3/1, 1/1, 1/3, and 1/6) are given in Fig. 8. Glucose conversion was not notable in a catalyst-free environment. Changing Mg/Al ratio did not affect the glucose conversion significantly except Mg-Al(6:1). The lowest glucose conversion (8.5%) was obtained with Mg-Al(6:1). Other catalysts exhibited approx. 16–18% conversions.

The formic acid yields are given in Fig. 9. The highest FA yield (4.7%) and selectivity (29.4%) were obtained with Mg-Al(1:3) catalyst. The FA yield raised with the

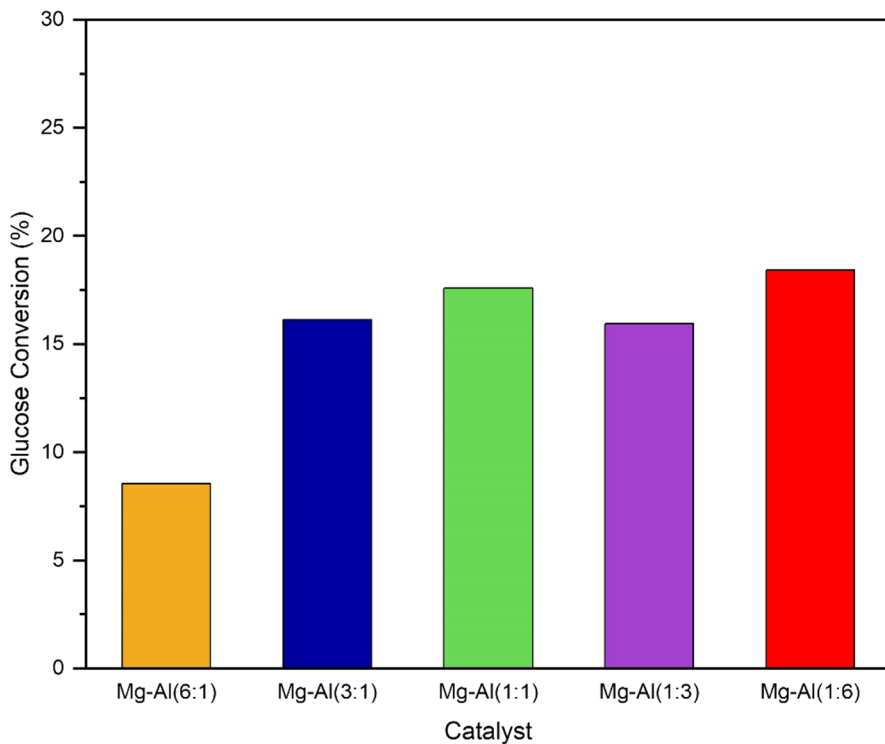


**Fig. 8** Glucose conversions of dried hydrotalcite-like catalysts with different Mg–Al ratios (Solvent: Ethanol, Temperature: 70°C, Time: 6 h, Catalyst/Glucose:1/2, 2% Glucose Loading, 250% H<sub>2</sub>O<sub>2</sub> solution)

increased in the aluminum ratio (except Mg–Al(1:6)). Unexpectedly, no formic acid was produced by Mg–Al(1:6) catalyst.

In literature, some alkaline earth metal salts (MgCl<sub>2</sub> or CaCl<sub>2</sub>) were found very effective to oxidize the sugar but not effective alone in formic acid production [34]. The transition metals (FeCl<sub>3</sub>, CrCl<sub>3</sub> or MnCl<sub>2</sub> and AlCl<sub>3</sub>) were more selective for organic acids, especially formic acid [34]. The basic medium or alkali metals contribute to the conversion of glucose, but formic acid is formed by the transition metals in heterogeneously catalyzed oxidation. The results were clearly seen in Figs. 8 and 9.

### Activity tests of calcined hydrotalcite-like catalysts

The glucose conversions of calcined hydrotalcite-like catalysts with different Mg/Al ratios (6/1, 3/1, 1/1, 1/3, and 1/6) are given in Fig. 10. The glucose conversion increased with reaction time in all catalysts. Increasing the Mg/Al ratio enhanced the conversion (except Mg–Al(6:1)). The highest conversion was obtained as 65.1% with Mg–Al(3:1). As compared with the dried samples, calcined ones were seen much more active (approximately 4 times) in the oxidation of glucose.

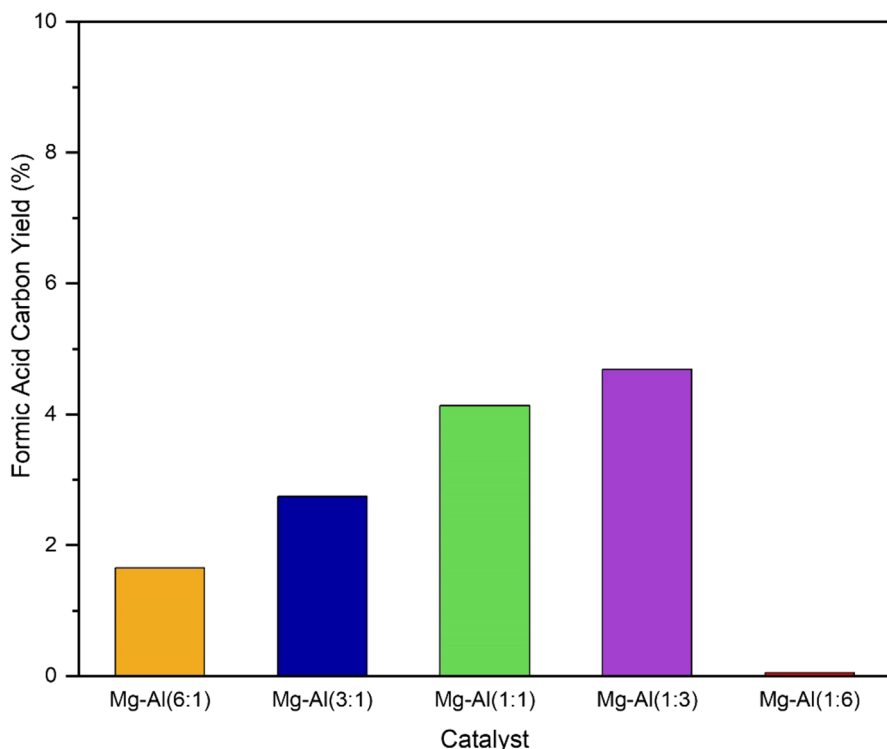


**Fig. 9** Formic acid carbon yield of dried hydrotalcites with different Mg–Al ratios (Solvent: Ethanol, Temperature: 70 °C, Time: 6 h, Catalyst/Glucose: 1/2, 2% Glucose Loading, 250% H<sub>2</sub>O<sub>2</sub> Solution).

Because, strong basic centers on the surfaces of hydrotalcites—formed during the calcination process—accelerated the oxidation of glucose and increased stability of catalysts [40].

Time-dependent formic acid carbon selectivities of the calcined catalysts are shown in Fig. 11. The selectivities of formic acid increased slightly up to 4 h with the decrease in the Mg/Al ratio. After 4th hour, FA yield significantly increased over Mg–Al(1:3) and Mg–Al(1:6) and reached to 99 and 74%, respectively. These results indicated that the breakdown of hydrogen peroxide formed O radicals; these radicals reacted with glucose molecules in virtue of Mg metal to produce intermediates [43] until the 4th hour of the reaction. These products were converted then into formic acid on the centers where the Al atom and CO<sub>3</sub><sup>2-</sup> ions were located [43].

As mentioned in Fig. 1, as the Mg/Al ratio reduced, the materials moved away from the hydrotalcite structure and the crystal density shifted toward magnesium aluminates, which was very effective in formic acid production. Meanwhile, Mg–Al(1:3) and Mg–Al(1:6) catalysts preserved the Metal-OH and CO<sub>3</sub><sup>2-</sup> groups in their structure even after the calcination, compared to other hydrotalcites (Fig. 2). Based on these performances, the rest of the tests were continued with Mg–Al(1:3).

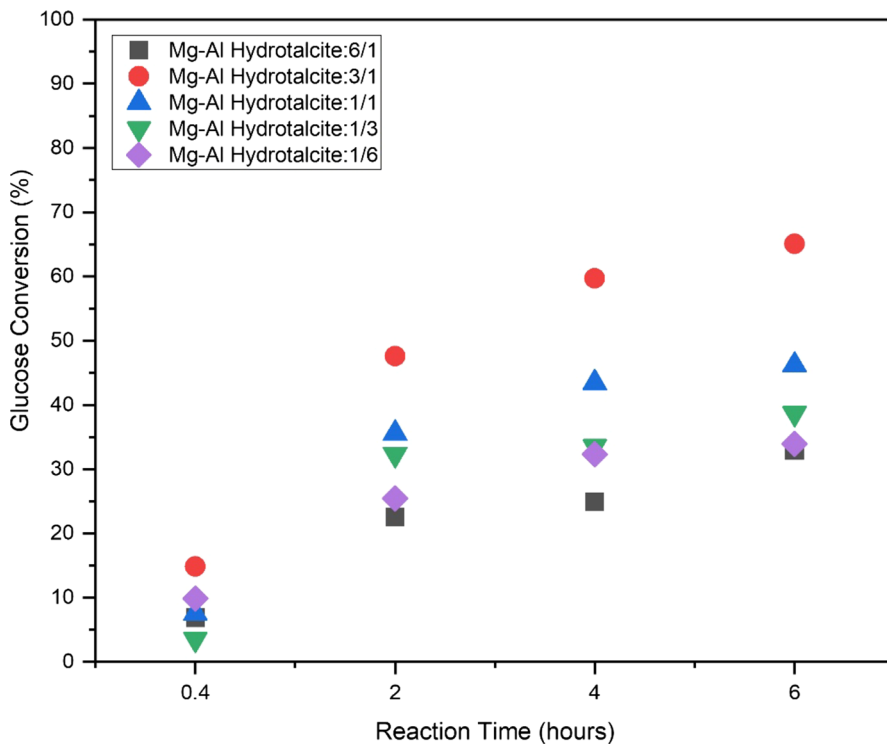


**Fig. 10** Glucose conversion over calcined hydrotalcites prepared at different Mg–Al ratios (Solvent: Ethanol, Temperature: 70 °C, Catalyst/Glucose:1/2, 2% Glucose Loading, 250% H<sub>2</sub>O<sub>2</sub> Solution, Catalyst Calcination Temperature: 450 °C).

### Effect of calcination temperature on glucose conversion and formic acid selectivity

Calcination of prepared catalysts improved the activities and formic acid selectivities. Mg–Al(3:1) was determined as a model catalyst in order to examine the effect of calcination temperature and the effect of crystal phase on catalytic activity and formic acid selectivity. This catalyst was calcined at different temperatures (450 °C, 650 °C, and 900 °C). The glucose conversion, formic acid carbon yields, and selectivities of Mg–Al(3:1)-450, Mg–Al(3:1)-650, and Mg–Al(3:1)-900 catalysts are given in Fig. 12. The highest glucose conversion (49.3%) was obtained with Mg–Al(3:1)-650 catalyst, but the highest formic acid carbon yield (7.43%) and selectivity (17.32%) were obtained with Mg–Al(3:1)-900 which was slightly higher than Mg–Al(3:1)-450. Therefore, considering the amount of energy consumption, the optimum calcination temperature was determined as 450 °C.

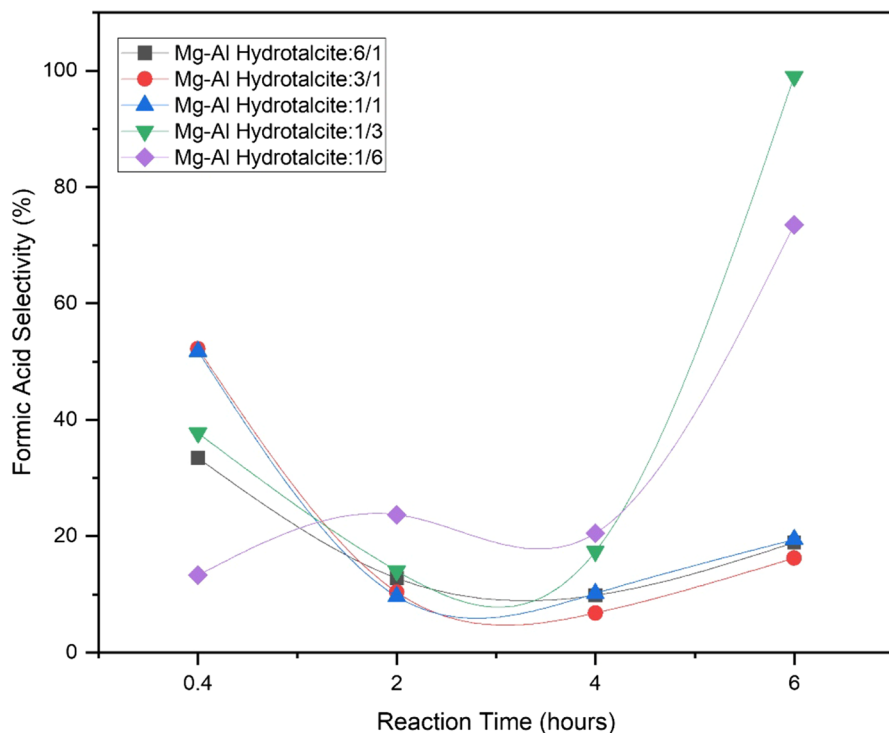


**Fig. 11** Formic acid selectivity of calcined hydrotalcites with different Mg–Al ratios (Solvent: Ethanol, Temperature: 70 °C, Catalyst/Glucose:1/2, 2% Glucose Loading, 250% H<sub>2</sub>O<sub>2</sub> Solution, Catalyst Calcination Temperature: 450 °C)

### Effect of solvent type on glucose conversion and formic acid selectivity

In the literature studies, it has been observed that the type of solvent may affect the oxidation products distribution. The most suitable solvents for oxidation were determined as alcohols (ethanol) and water. For this reason, aqueous ethanol (EtOH) solutions in different proportions (100%, 50% and 0%, (EtOH-Water)) were prepared and their effects on glucose conversion and formic acid selectivities were investigated. Results are given in Figs. 13 and 14. The presence of water did not affect the catalytic activity (~40%) significantly where formic acid was maximized with the absence of water. The highest selectivity (99%), without any by-product, was obtained in 100% ethanol medium. It was previously reported the formation of the carboxylic acid intermediates during glucose oxidation [7]. Decarboxylation of these intermediates favors the formation of CO<sub>2</sub>, especially in aqueous mediums. When an alcohol is used as a solvent, the formation of CO<sub>2</sub> during the reaction is prevented and formic acid yield is improved [7]. In addition, as a result of the reaction of aldehydes (glucose) with alcohols (ethanol), hemiacetal structures are formed and the conversion of glucose to non-formic

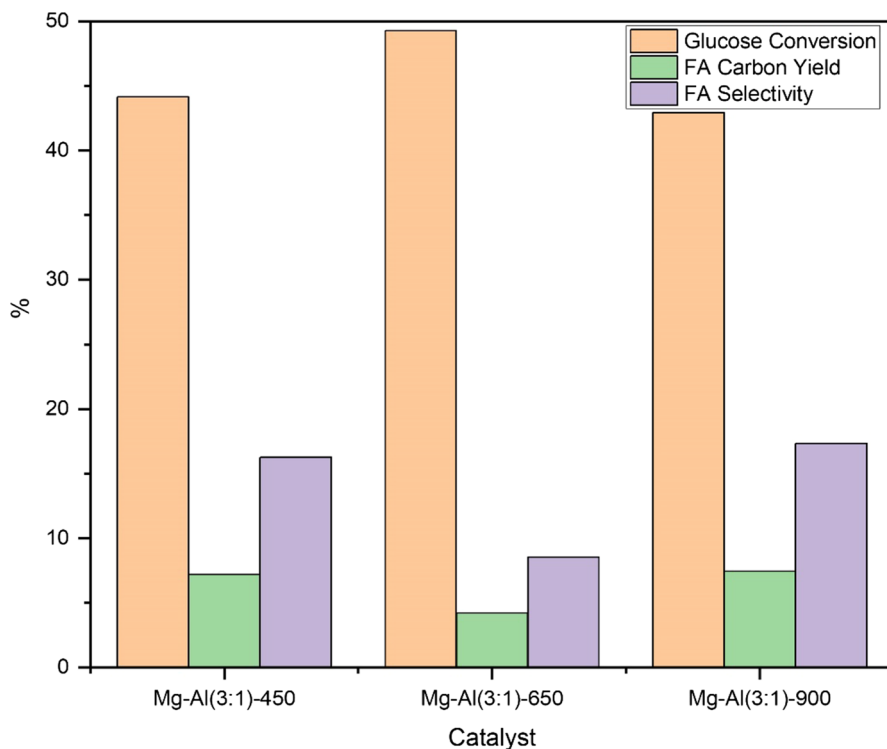


**Fig. 12** Glucose conversion, formic acid carbon yield, and formic acid selectivity of Mg–Al(3:1) catalyst calcined at different temperatures (Solvent: Ethanol, Temperature: 70 °C, Time: 6 h, Catalyst/Glucose:1/2, 2% Glucose Loading, 250% H<sub>2</sub>O<sub>2</sub> Solution)

acid carboxylic acids (acetic acid, glycolic acid) are prevented [54]. Thus, formic acid selectivity increases significantly in ethanol medium.

### Effect of reaction temperature on glucose conversion and formic acid selectivity

The time-dependent glucose conversions at different temperatures are given in Fig. 15. The reaction was carried out at three different temperatures (30 °C, 50 °C, and 70 °C). The highest temperature was determined as 70 °C considering decomposition of H<sub>2</sub>O<sub>2</sub> above 70 °C and boiling point of EtOH [55]. Although the oxidation reaction was exothermic, glucose conversion (9.6%, 25.0%, and 38.7%) increased with temperature by the increase in molecular motion and surface activity. The time trends of conversions and the differences between conversion lines at each time point indicated the accuracy of the oxidation results.

The selectivities of formic acid obtained at different temperatures are shown in Fig. 16. The highest product selectivity (99%) was obtained at the highest temperature where the lowest product selectivity (29.6%) was at the lowest reaction temperature. A huge difference in selectivities was observed between 70 and 50 °C.



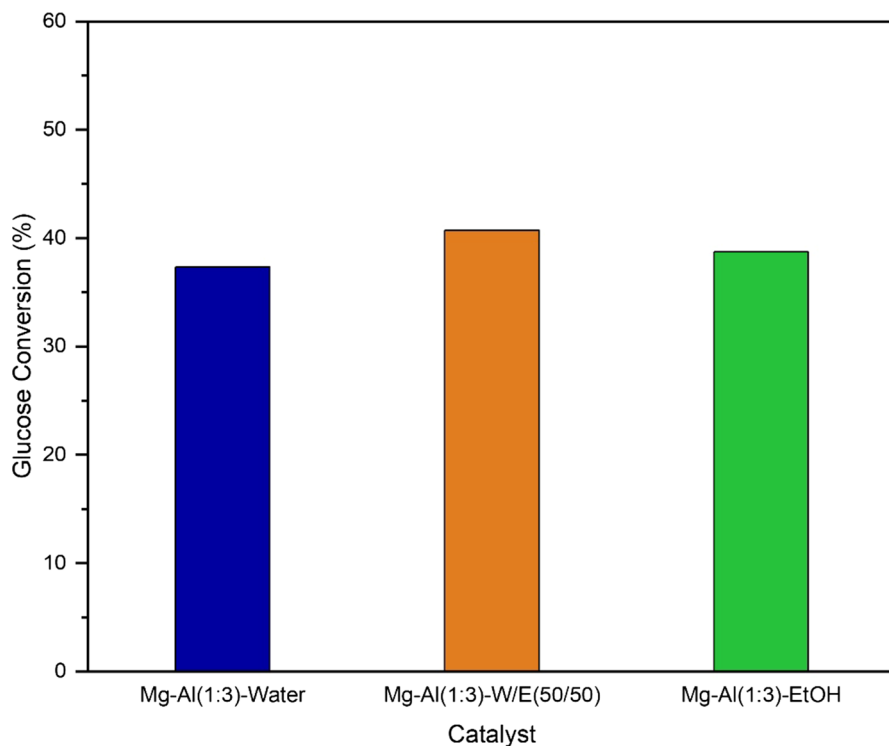


**Fig. 13** Glucose conversion of Mg–Al(3:1) catalyst calcined in the different reaction medium (Temperature: 70 °C, Time: 6 h, Catalyst/Glucose: 1/2, 2% Glucose Loading, 250% H<sub>2</sub>O<sub>2</sub> Solution)

Although the temperature difference is only 20 °C, the slight increase in temperature could be changed the mechanism. It was noticed that the selectivity at 30 °C was higher than at 50 °C. This was due to the formation of CO<sub>2</sub> that starts after 30 °C.

### Effect of catalyst/glucose ratio on glucose conversion and formic acid production

Effects of catalyst/glucose (1/5, 1/2, and 1/1) ratio on glucose conversion were investigated. The time-dependent glucose conversion amounts of different catalyst/glucose ratios are given in Fig. 17. The glucose conversion increased with the amount of catalyst depending on the increase in the active sites per glucose molecule. The highest glucose conversion (71.9%) was obtained when the catalyst/glucose ratio was chosen as 1/1.

The effect of different catalyst/glucose (1/5, 1/2, and 1/1) ratios on formic acid selectivity was examined (Fig. 18). When the amount of catalyst was increased, formic acid selectivity decreased from 99 to 64.7%. This was attributed to the formation of side reactions and the high number of active centers caused the conversion of glucose into other products. Formic acid formation at G/C = 1/5 was not remarkable. This may be due to the insufficient number of active sites

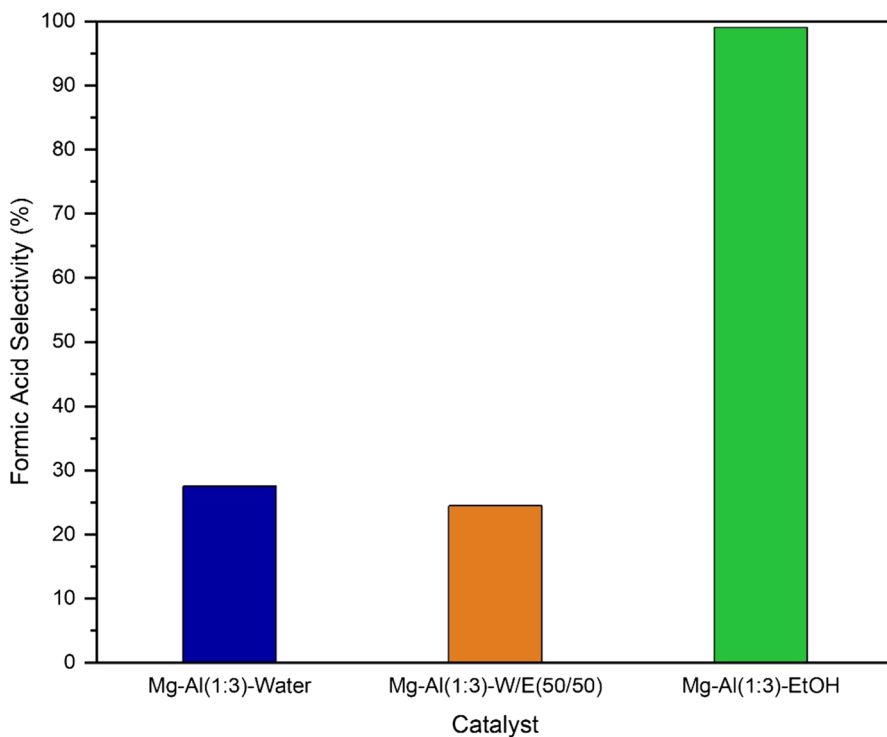


**Fig. 14** Formic acid selectivities of Mg–Al(3:1) catalyst in different reaction mediums (Temperature: 70 °C, Time: 6 h, Catalyst/Glucose: 1/2, 2% Glucose Loading, 250% H<sub>2</sub>O<sub>2</sub> Solution)

per glucose molecule, instantaneous occupation of these sites, and undesired reactions between unbonded glucose molecules and solvent, products, etc.

### Catalyst stability

Mg–Al(1:3) catalyst were tested in a series of recycle reactions and the re-used catalyst after the 1st reaction was analyzed by XRD. XRD patterns of the used catalyst and series activity results are given in Figs. 19 and 20, respectively. Recovered catalysts after each run were washed and calcined for the consecutive reaction cycles. Glucose conversion slightly reduced after 3rd run; however it was significantly decreased after the 4th use. XRD results of the used catalyst exhibited the same crystal structure with higher intensities. This could be due to the enlarging of MgO crystals during the reaction. Dramatic drop in the activity after 4th run could be attributed to the formation of humins and deactivation of the active sites by these molecules.

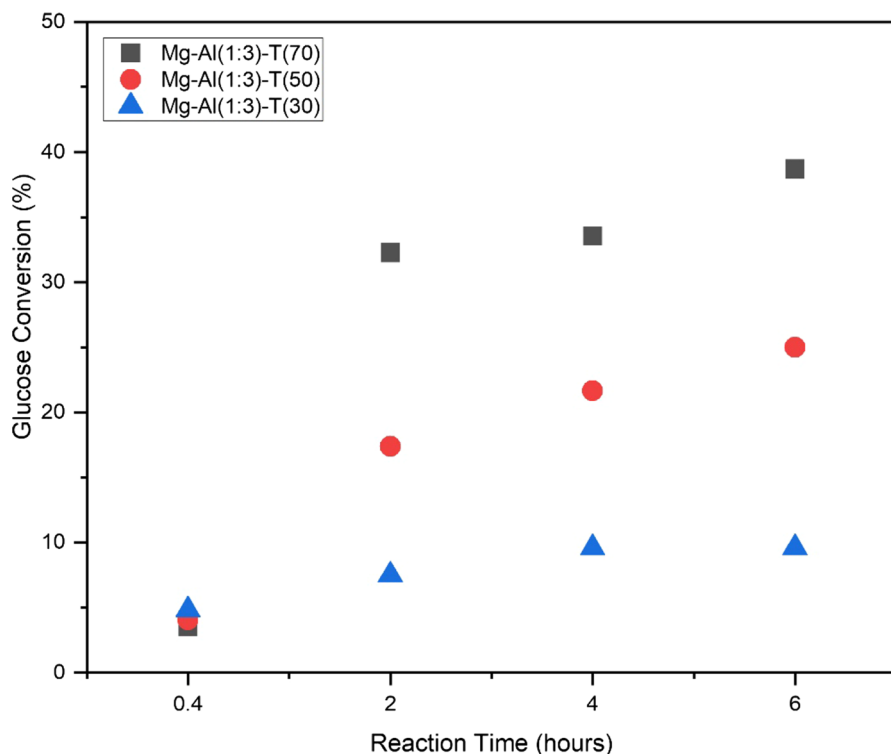


**Fig. 15** Glucose conversion of Mg–Al(1:3) calcined hydrotalcites at different reaction temperatures (Solvent: Ethanol, Catalyst/Glucose:1/2, 2% Glucose Loading, 250% H<sub>2</sub>O<sub>2</sub> Solution, Catalyst Calcination Temperature: 450 °C)

## Conclusions

Selective oxidation of glucose to formic acid under base free mild conditions was successfully achieved over hydrotalcite-like catalysts. Synthesized catalysts exhibited high glucose conversions (~60% over Mg–Al (3:1)) and extremely high formic acid selectivities (~99% over Mg–Al (1:3)) in ethanol by using H<sub>2</sub>O<sub>2</sub> as oxidant at 70 °C. Densities of the hydrotalcite crystals and average pore diameters of the catalysts reduced as Mg/Al ratio increased, while surface area and amount of metal-OH bonds increased. Mg–Al (1:3) had most narrow pore size distributions that indicated the more uniformly packing of this material compared to others. Mg–Al (1:3) provided the highest formic acid yield and selectivity

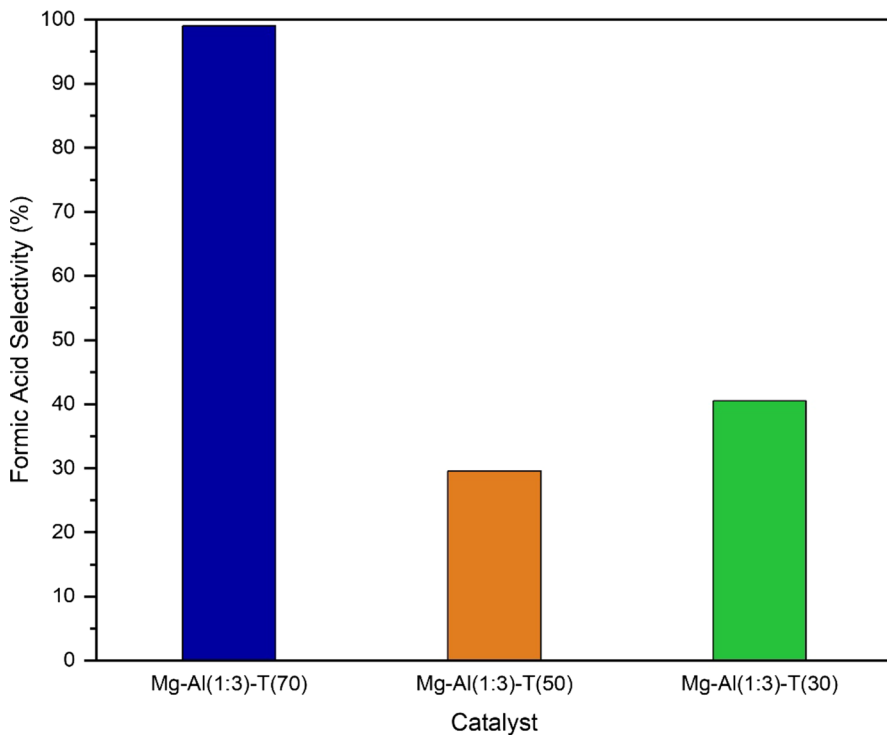


**Fig. 16** Formic acid selectivity of Mg–Al(1:3) calcined hydrotalcites at different reaction temperatures (Solvent: Ethanol, Reaction time: 6 h, Catalyst/Glucose:1/2, 2% Glucose Loading, 250% H<sub>2</sub>O<sub>2</sub> Solution, Catalyst Calcination Temperature: 450 °C)

(37% FA yield and 99% FA selectivity) among the all synthesized catalysts. The calcination process significantly improved the catalytic activities of the catalysts (~4X in conversion and ~7X in yield). The effect of water/ethanol ratio was also demonstrated. Presence of water in solvent significantly decreased the FA yield since water favored the formation of CO<sub>2</sub>. A dramatic drop in FA selectivity was observed when the reaction temperature was reduced to 50 °C due to the reaction mechanism. Doubling the catalyst/glucose ratio increased the conversion by 84% while lowering the selectivity by 30%.

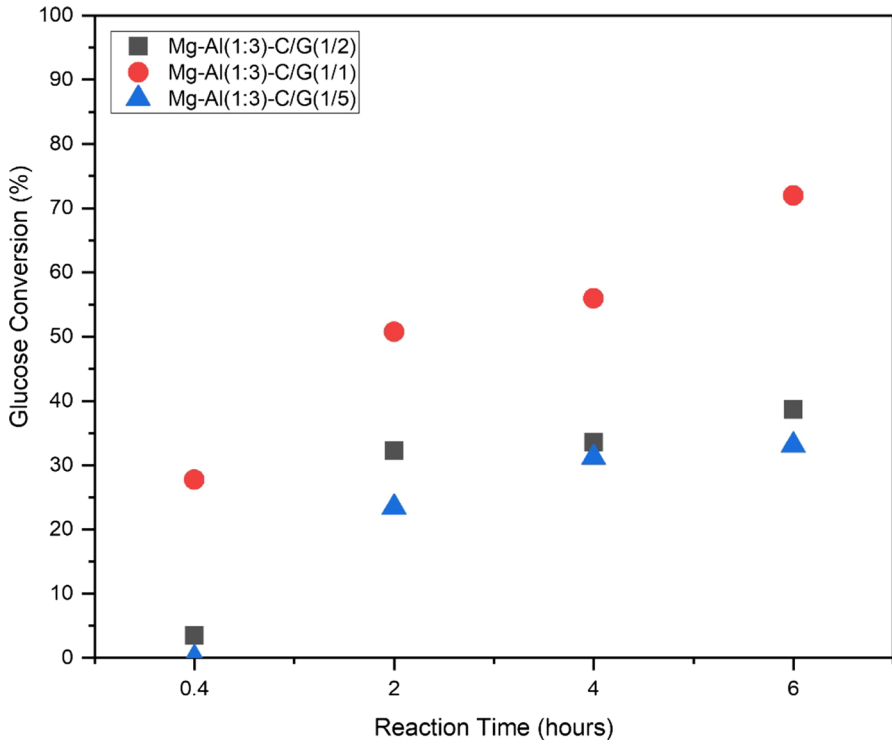


**Fig. 17** Glucose conversion of Mg–Al(1:3) calcined hydrotalcites at different catalyst/glucose ratios (Solvent: Ethanol, Reaction Temperature: 70 °C, 2% Glucose Loading, 250% H<sub>2</sub>O<sub>2</sub> Solution, Catalyst Calcination Temperature: 450 °C)

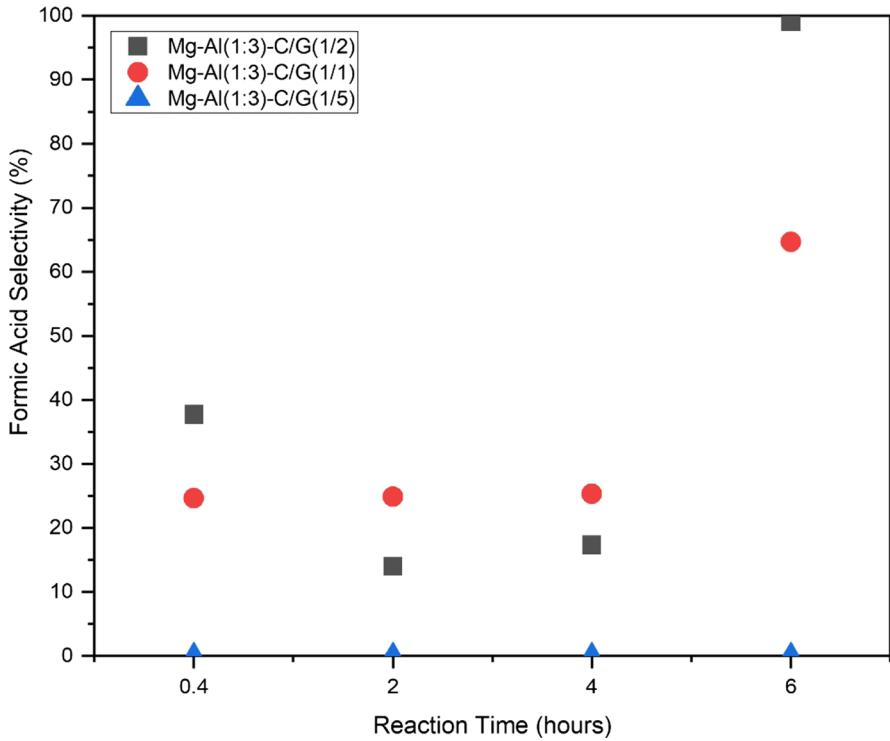


**Fig. 18** Formic acid selectivity of Mg–Al(1:3) calcined hydrotalcites at different catalyst/glucose ratios (Solvent: Ethanol, Reaction Temperature: 70 °C, 2% Glucose Loading, 250% H<sub>2</sub>O<sub>2</sub> Solution, Catalyst Calcination Temperature: 450 °C)

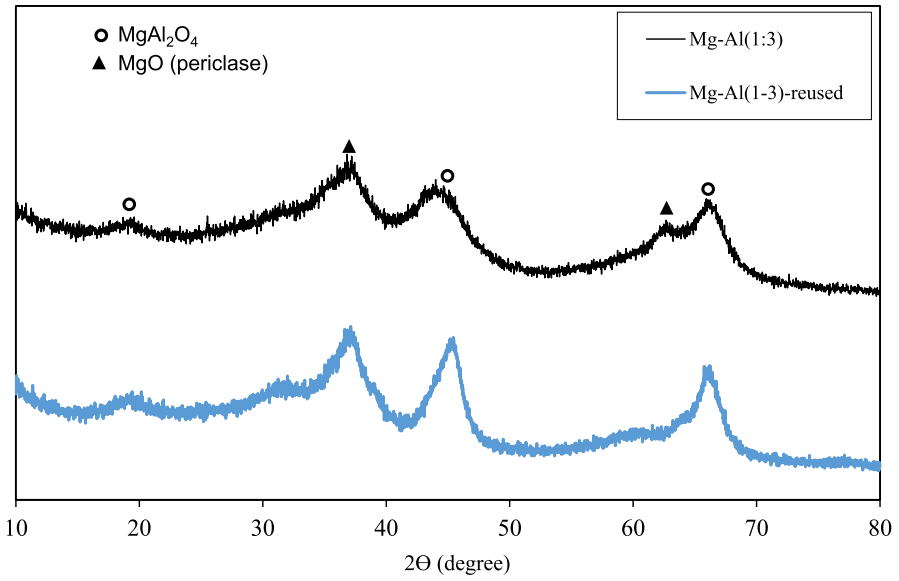


**Fig. 19** XRD patterns of fresh and re-used Mg–Al (1:3) HT catalyst

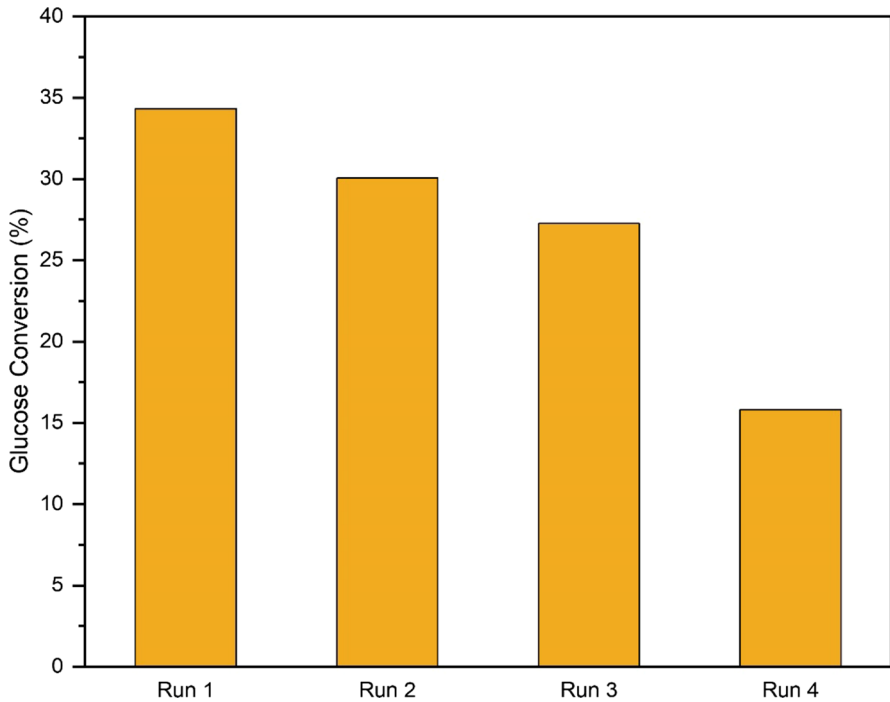


**Fig. 20** Recycle reaction results of Mg–Al (1:3) HT catalyst

**Acknowledgements** This work was mainly financially supported by Research Fund of Usak University (2019/DTS005) and Regional Development Program. All of the synthesized catalysts were characterized in Recep Tayyip Erdoğan University Central Research Laboratory Application and Research Center, Rize, Turkey. We are grateful to all team staff for their support. Hülya A. Kılıç is grateful for the support provided by Higher Education Institution (YOK 100/2000, Fuels (fossil and bio-) and Combustion) PhD funding program.

**Author contributions** The manuscript was written through contributions of all authors. All authors have given approval to the final version of the manuscript.

**Funding** This work was mainly financially supported by Research Fund of Usak University (2019/DTS005) and Regional Development Program.

## Declarations

**Conflict of interest** The authors declare no competing financial interest.

## References

1. T. Thananathanachon, T.B. Rauchfuss, *Angew. Chemie - Int. Ed.* **49**, 6616 (2010)
2. S.D. Sheet, *I.C.I.S. Chem. Bus.* **1**, 1 (2017)
3. J. Zhao, M. Liu, G. Fan, L. Yang, F. Li, *Ind. Eng. Chem. Res.* **60**, 5826 (2021)
4. S. Fukuzumi, T. Kobayashi, T. Suenobu, *J. Am. Chem. Soc.* **132**, 1496 (2010)
5. X. Li, X. Ma, F. Shi, Y. Deng, *Chemsuschem* **3**, 71 (2010)
6. B. Loges, A. Boddien, H. Junge, J.R. Noyes, W. Baumann, M. Beller, *Chem. Commun.* **28**, 4185 (2009)
7. Z. Tang, W. Deng, Y. Wang, E. Zhu, X. Wan, Q. Zhang, Y. Wang, *Chemsuschem* **7**, 1557 (2014)
8. F.R. Tao, C. Zhuang, Y.Z. Cui, J. Xu, *Chinese Chem. Lett.* **25**, 757 (2014)
9. J. Yun, F. Jin, A. Kishita, K. Tohji, H. Enomoto, in *J. Phys. Conf. Ser.* (2010)
10. Z. Qiao, Z. Wang, C. Zhang, S. Yuan, Y. Zhu, J. Wang, *AIChE J.* **59**, 215 (2012)
11. F. Joó, *Chemsuschem* **1**, 805 (2008)
12. F. Wang, Y. Wang, F. Jin, G. Yao, Z. Huo, X. Zeng, Z. Jing, *Ind. Eng. Chem. Res.* **53**, 7939 (2014)
13. N.V. Gromov, O.P. Taran, I.V. Delidovich, A.V. Pestunov, Y.A. Rodikova, D.A. Yatsenko, E.G. Zhzhina, V.N. Parmon, *Catal. Today* **278**, 74 (2016)
14. C. Wang, X. Chen, M. Qi, J. Wu, G. Gözaydin, N. Yan, H. Zhong, F. Jin, *Green Chem.* **21**, 6089 (2019)
15. K. Li, L. Bai, P.N. Amaniampong, X. Jia, J.M. Lee, Y. Yang, *Chemsuschem* **7**, 2670 (2014)
16. B. Jin, G. Yao, X. Wang, K. Ding, F. Jin, *A.C.S. Sustain. Chem. Eng.* **5**, 6377 (2017)
17. J. Ahlqvist, *Formic and levulinic acid from cellulose via heterogeneous catalysis (2013)*.
18. T. Moreno, G. Kouzaki, M. Sasaki, M. Goto, M.J. Cocero, *Carbohydr. Res.* **349**, 33 (2012)
19. J. Albert, *Faraday Discuss.* **202**, 99 (2017)
20. Z. Babaei, R. Yazdanpanah Esmaeilabad, N. Orash, and A. Najafi Chermahini, *Biomass Convers. Biorefinery* **2**, (2020).
21. S. Ponce, S. Wesinger, D. Ona, D. A. Streitwieser, and J. Albert, *Biomass Convers. Biorefinery* (2021).
22. Y. Qu, Y. Zhao, S. Xiong, C. Wang, S. Wang, L. Zhu, L. Ma, *Energy Fuels* **34**, 11041 (2020)
23. Y. Feng, M. Zuo, T. Wang, W. Jia, X. Zhao, X. Zeng, Y. Sun, X. Tang, T. Lei, L. Lin, *J. Taiwan Inst. Chem. Eng.* **96**, 431 (2019)
24. U. Tyagi and N. Anand, *Biomass Convers. Biorefinery* (2020).
25. S. Dutta, *Biomass Convers. Biorefinery* (2021).
26. F. Huang, T. Jiang, H. Dai, X. Xu, S. Jiang, L. Chen, Z. Fei, P.J. Dyson, *Catal. Letters* **150**, 2599 (2020)
27. P.V. Rathod, R.B. Mujmule, W.-J. Chung, A.R. Jadhav, H. Kim, *Catal. Letters* **149**, 672 (2019)
28. B. Guo, L. He, G. Tang, L. Zhang, L. Ye, B. Yue, S.C.E. Tsang, H. He, *Chinese. J. Catal.* **41**, 1248 (2020)



29. V.V. Ordonsky, V.L. Sushkevich, J.C. Schouten, J. Van Der Schaaf, T.A. Nijhuis, *J. Catal.* **300**, 37 (2013)
30. Y. Hou, M. Niu, W. Wu, *Ind. Eng. Chem. Res.* **59**, 16899 (2020)
31. D. Garcés, E. Díaz, S. Ordóñez, *Ind. Eng. Chem. Res.* **56**, 5221 (2017)
32. F. Jin, J. Yun, G. Li, A. Kishita, K. Tohji, H. Enomoto, *Green Chem.* **10**, 612 (2008)
33. F. Jin, H. Enomoto, *Energy Environ. Sci.* **4**, 382 (2011)
34. T. Lu, Y. Hou, W. Wu, M. Niu, S. Ren, Z. Lin, V.K. Ramani, *Fuel* **216**, 572 (2018)
35. Y. Önal, S. Schimpf, P. Claus, *J. Catal.* **223**, 122 (2004)
36. A. Mafta, L. Ulrich, J. Kornecki, R. Fernandez-Lafuente, P. Tardioli, M. Ribeiro, *Catalysts* **9**(8), 657 (2019). <https://doi.org/10.3390/catal9080657>
37. S. Franz, N.D. Shcherban, I. Bezverkhy, S.A. Sergiienko, I.L. Simakova, T. Salmi, D.Y. Murzin, *Res. Chem. Intermed.* **47**, 2573 (2021)
38. J. Albert, R. Wölfel, A. Bösmann, P. Wasserscheid, *Energy Environ. Sci.* **5**, 7956 (2012)
39. F. Cavani, F. Trifirò, A. Vaccari, *Catal. Today* **11**, 173 (1991)
40. D. Kwon, J.Y. Kang, S. An, I. Yang, J.C. Jung, *J. Energy Chem.* **46**, 229 (2020)
41. V.R. Choudhary, P.A. Chaudhari, V.S. Narkhede, *Catal. Commun.* **4**, 171 (2003)
42. A.V.P. Lino, E.M. Assaf, J.M. Assaf, *Catal. Today* **289**, 78 (2017)
43. R. Sato, H. Choudhary, S. Nishimura, K. Ebitani, *Org. Process Res. Dev.* **19**, 449 (2015)
44. M.D. Özcan, O. Özcan, M.E. Kibar, A.N. Akin, *J. Fac. Eng. Archit. Gazi Univ.* **34**, 1127 (2019)
45. O.V. Larina, P.I. Kyriienko, N.D. Shcherban, P.S. Yaremov, D.Y. Balakin, I. Khalakhan, K. Vel-truská, S.O. Soloviev, S.M. Orlyk, *Ind. Eng. Chem. Res.* **60**, 11964 (2021)
46. M.A. López-Martínez, I. Melián-Cabrera, *Ind. Eng. Chem. Res.* **60**, 11848 (2021)
47. P. Völs, S. Hilbert, B. Störr, N. Bette, A. Lißner, J. Seidel, F. Mertens, *Ind. Eng. Chem. Res.* **60**, 5114 (2021)
48. C.E. Daza, C.R. Cabrera, S. Moreno, R. Molina, *Appl. Catal. A Gen.* **378**, 125 (2010)
49. W.T. Reichle, *Solid State Ionics* **22**, 135 (1986)
50. G. Zi, Z. Yan, Y. Wang, Y. Chen, Y. Guo, F. Yuan, W. Gao, Y. Wang, J. Wang, *Carbohydr. Polym.* **115**, 146 (2015)
51. R.C. Zeng, X.T. Li, Z.G. Liu, F. Zhang, S.Q. Li, H.Z. Cui, *Mater. Sci.* **9**, 355 (2015)
52. C.L. Caldeira, V.S.T. Ciminelli, K. Osseo-Asare, *Geochim. Cosmochim. Acta* **74**, 1777 (2010)
53. B. Kostura, D. Matýšek, J. Kukutschová, J. Leško, *Ann. Chim. Sci. Des Mater.* **37**, 11 (2012)
54. J. Liu, Z. Du, Y. Yang, T. Lu, F. Lu, J. Xu, *Chemsuschem* **5**, 2151 (2012)
55. B. Sarkar, C. Pendem, L.N. Sivakumar Konathala, R. Tiwari, T. Sasaki, R. Bal, *Chem. Commun.* **50**, 9707 (2014)

**Publisher's Note** Springer Nature remains neutral with regard to jurisdictional claims in published maps and institutional affiliations.

Springer Nature or its licensor holds exclusive rights to this article under a publishing agreement with the author(s) or other rightsholder(s); author self-archiving of the accepted manuscript version of this article is solely governed by the terms of such publishing agreement and applicable law.